sciendo INTERNATIONAL JOURNAL ON SMART SENSING AND INTELLIGENT SYSTEMS

Article | DOI: 10.2478/ijssis-2022-0009 Issue 1 | Vol. 15 (2022)

The ordinary negative changing refractive index for estimation of optical confinement factor

Ahmad S. Abdullah*,
Sadeq Adnan Hbeeb

Department of Communications, College of Engineering, University of Diyala, Iraq.

*E-mail: ahmed.alogaidi28@gmail.com

This paper was edited by Subhas Chandra Mukhopadhyay.

Received for publication December 23, 2021.

Abstract

The electro-optic effect is considered very important in optical communication systems. The small optical confinement factor is attributed to the weak overlap between the electric field and optical wave and hence the optical signal is not efficiently modulated. In this paper, the problem of the small optical confinement factor in the Mach–Zehnder modulator based on lithium niobate (LN) which is deeply studied. The data were analyzed through a proposed mathematical model to explain the relationship between the change in the ordinary negative refractive index and the confinement factor. The system is improved using a small length of the modulator arm as only 3 to 8 μm, low driving power of about 4 V/μm, a large change in the negative ordinary refractive index of about—0.2×10^{-7}, and a compact optical modulator. This can reflect a strong optical confinement factor when the electric field is applied to the electrodes of the optical modulator.

Keywords

Electro-optic effect, Lithium niobate LN, Mach–Zehnder modulator MZM, Optical confinement factor.

Introduction

The optical properties of materials vary under the influence of an electro-optic caused by an electrical field which is progressively changing with the optical light. The applied electric field changes the refractive index of the exposed material using an electro-optic effect as illustrated in Figure 1 (Bea and Teich, 1991).

The performance of many devices can be degraded under such exposure. For instance, the size of the Mach–Zehnder modulator (MZM) becomes larger (i.e., the length of branches MZM is increased), the bending losses of waveguides are greater, the *Q*-factor is diminished, and the size of the resonators is enlarged (Qi and Li, 2020). These performance degradations are attributed to the weak optical confinement factor (i.e., the overlap is small) resulting from the low relative refractive index variance (Yi-Yan, 1983; Korkishko et al., 1996; Cai et al., 2016). Some materials possess optical and structural properties that make them usable in many fields such as hydrogen production and wastewater treatment (Scharnberg et al., 2020). There is research concerned with studying the optical, structural, and electronic properties of some materials (Akhtar, 2022). Lithium niobate (LN) indicates the possibility to improve the overall performance of electro-optic modulators at the expense of its environmental properties. Examples of these improvements are powerful linear effect (i.e., Pockels effect), enormous transparency window, massive electro-optic coefficient (30 pm/V), and the stability of the temperature are at its best (Wooten et al., 2000). Thus, the low refractive index with large switching voltage–length product ($V\pi \cdot L$, usually >10 V cm (Janner et al., 2009)) can create a problem for diffused or proton-exchange waveguide of commercial bulk LN modulators because it reflects a weak optical confinement factor. A standard length of a lithium niobate insulator (LNOI) photonic waveguide is much less than 1 μm^2, which helps reach a small

Open Access. Published by Sciendo. BY-NC-ND
© 2022 Authors. This work is licensed under the Creative Commons Attribution-Non-Commercial-NoDerivs 4.0 License https://creativecommons.org/licenses/by-nc-nd/4.0/

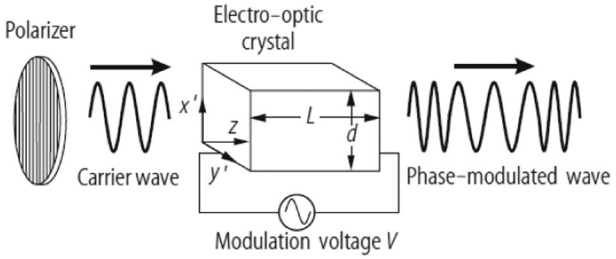


Figure 1: Applied electric field along z-direction changes the refractive index of crystal.

mode dimension and a strong optical confinement factor (Janner et al., 2009; Poberaj et al., 2012; Chang et al., 2016; Fathpour, 2017; Boes et al., 2018). This can coincide with the overlap between optical and electrical fields as a great performance of overlap and reduction switching voltage–length product (Xu et al., 2019). Furthermore, this strategy opens new levels of overall performance improvements for LN modulators due to a strong optical confinement factor and a large relative refractive index difference (Guarino et al., 2007; Janner et al., 2009; Poberaj et al., 2012; Chen et al., 2014; Jin et al., 2015; Rao et al., 2016; Chang et al., 2017; Rao and Fathpour, 2017; Boes et al., 2018; Mercante et al., 2018; Wang et al., 2018; Weigel et al., 2018; He et al., 2019; Xu et al., 2020). In hybrid LN-Si (silicone) electro-optic modulator (EOM), the performance of the LN overlap is 81%, and Si is 5% (Weigel et al., 2018; Wang et al., 2019), while the oxide SiO_2 includes the remaining of the light. The performance of the overlap (i.e., strong optical confinement factor) can be increased by etching the thin-film LN (He et al., 2019) as demonstrated in Figure 2. Assuming the process is flawless. Some developers use a variety of methods to detect defects resulting from manufacturing errors, such as automatic visual inspection (Priscilla et al., 2020).

In the integrated metal-diffused, the optical waveguides own a weak optical confinement factor that restricts an electro-optic exchange as a result of the lower efficiency of an electro-optic modulation and large footprints of devices (Priscilla et al., 2020). Lately, a larger optical confinement factor (big overlap) has been achieved using a uniform thin-film LN modulator integration that leads to enhancements in terms of compactness, information measure, and energy potency. This interesting technique has attracted multiple studies presented in (Tavlykaev and Ramaswamy, 1999; Zenin et al., 2012; Zenin et al., 2017Alexander et al., 2018; DeVault et al., 2018; Deshpande et al., 2018; Thomaschewski et al., 2020). However, for commercial demand, the length of the branches is still relatively long within the limit of mm-scale, because the extraction is limited within an overlap of an electro-optic field (Priscilla et al., 2020). Moreover, a photonic crystal PC (crystal is a type of a barium titanate $BaTiO_3$) can be used as a confined device for optical light and utilized with LN-Si devices. Nonetheless, this technique has reflected a weak optical confinement factor (i.e., small overlap) because of the small amount of confined optical light (Roussey et al., 2006, 2007; Lu et al., 2012a). Indeed, this problem is solved using a film of smart-cut LN (Sulser et al., 2009; Lu et al., 2012b), where it utilized a $BaTiO_3$ PC structure in which the confined optical light has been magnified. This approach is named as high-speed PC modulator (Girouard et al., 2017). To design a small size system in micrometer is always challenging because of the required large enough confinement factor to consequently achieve

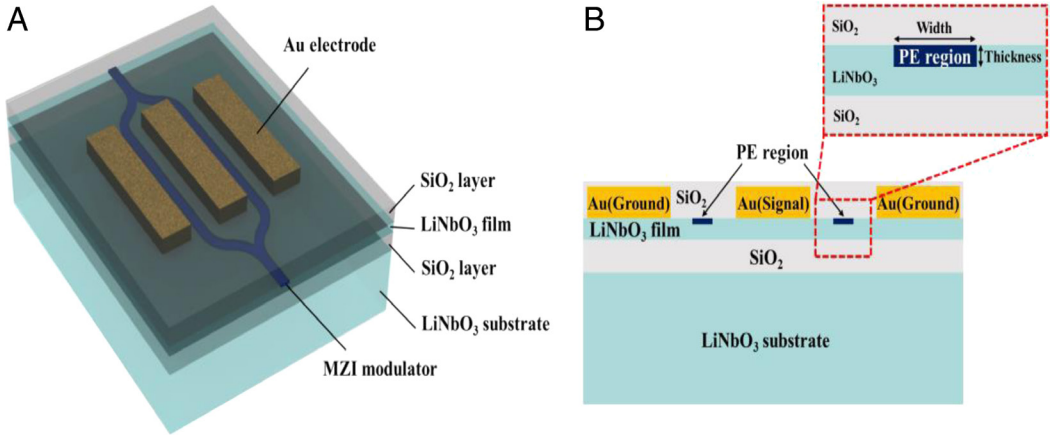


Figure 2: (a) A Mach–Zehnder interferometer modulator MZIM. (b) The cross-sectional diagram of the MZIM and the channel of the waveguides.

high-quality modulation. In this design, the variation value of the ordinary negative refractive index (–Δn), in which the power is –7, is good because it is close to previous results. In addition, the development of the system using as small as 3 to 8 μm length of the modulator arm, low-energy consumption of about 4 V/μm, a large negative ordinary relative refractive index difference of about—0.2 × 10^{-7}. Therefore, from the results of combining the optical light with the electric field, the system indicates a better overlap with a sufficiently large change in the negative ordinary refractive index.

Analytical model

This paper employs an electro-optic effect technique based on LN Mach–Zehnder modulator (MZM), as shown in Figure 3 and Table 1. This technique has reduced the electric field and minimized the length of arms to micrometer with suitable level of refractive index and strong optical confinement factor (i.e., a large overlap).

For the Mach–Zehnder interferometer (MZI), where the initial intensity of light Io in lum is modulated with the applied electric field *E* in V/m as follows (Figura, 2000):

$$E = E_o e^{i(Kx-wt)} \tag{1}$$

where E_o is the static electric field in V/m, *i* is the imaginary part, *K* is the wavenumber which equals $2\pi/\lambda$, λ is the optical wavelength in nm, *w* is the angular frequency in Hz, and *t* is the time domain in sec.

The optical wave is divided into two branches of the modulator with equal lengths and refractive indices. Since the optical path length through each branch is the same, it will have a constructive interference at the end of the arms where the waves

Table 1. Electro-optic coefficients (r_{33}), refractive index (n_o) and wavelengths (λ), for LN.4.

r_{33}(pm/V)	Wavelength (nm)	n_o	Reference
31	633	2.2864	(Casson et al., 2004)
25	1560	2.2108	(Casson et al., 2004)

are recombined (Figura, 2000). Figure 4 visualizes MZI electro-optic modulator based on $LiNbO_3$.

$$I = I_o cos^2\left(\frac{\Delta\phi}{2}\right) \tag{2}$$

$$E = E_o \cos\left(\frac{\Delta\phi}{2}\right) e^{i(Kx-wt)} \tag{3}$$

where, *I* is the output intensity in lum and Δϕ is the phase difference. Therefore, the ordinary refractive index changes Δn_0 that results from the applied electrical field in the direction of the extraordinary axis of the medium as follows (Figura, 2000):

$$\Delta n_o = -\frac{1}{2} n_o^3 r_{33} E \tag{4}$$

where n_0 is the ordinary refractive index, r_{33} is the electro-optic coefficient pm/V·r_{ij} represented by second rank tensor and r_{ij} is the matrix in which $i = 1, \ldots, 6$

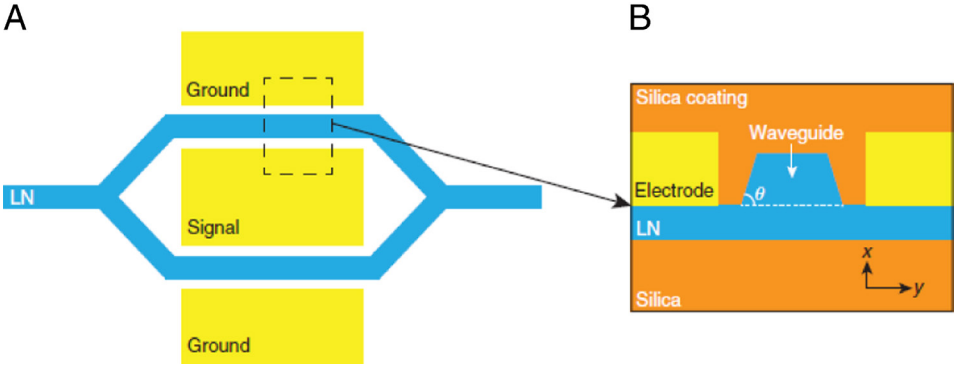


Figure 3: Integrated LN Mach-Zehnder modulator MZM: (a) top view and (b) cross-section area.

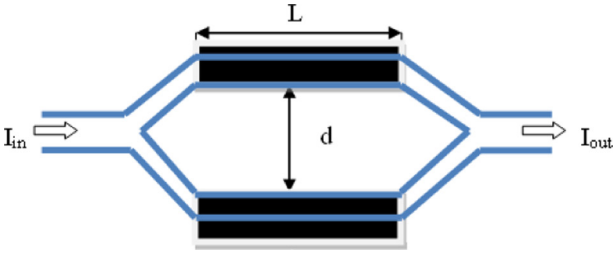


Figure 4: MZI electro-optic modulator based on $LiNbO_3$.

and j = 1, 2, 3, thus for r33, i = 3 and j = 3. When applying an external voltage on the arms, a phase difference ΔØ induces and the half-wave voltage (i.e., switching voltage) Vπ for MZM can then be calculated using (Figura, 2000):

$$\Delta\varnothing = \frac{\pi L r_{33} n_o^3 E}{\lambda} \tag{5}$$

where λ is the optical wavelength in nm, and L is the length of arms in μm.

$$V\pi = \frac{d\lambda}{L r_{33} n_o^3} \tag{6}$$

where d is the separation distance in between arms in μm. Moreover, the equation of MZM shows that the incident laser light splits into two components, I_{o1} and I_{o2}, that separate optical path and combined again at the last part of the device as optical power (i.e. $I_2 = I_{o1} + I_{o2}$) a, and I_1 = electro-optical input power (Luff et al., 1998; Hagn, 2001). Thus,

$$\frac{2I_1}{I_2} = -\frac{4\Delta n_o}{r_{33}\Gamma n_o^3}\left[\left(-\frac{2\Delta n_o}{r_{33}\Gamma n_o^3} - 1\right) + \left(1 + \frac{2\Delta n_o}{r_{33}\Gamma n_o^3}\right)\cos\Delta\varnothing\right] + 1 \tag{7}$$

where I_1 is the input optical power in Watt, I_2 is the electro-optical output power in Watt, and Γ is the optical confinement factor (unitless).

$$\frac{2I_1}{I_2} = -\frac{4\Delta n_o}{r_{33}\Gamma n_o^3}\left[-\frac{2\Delta n_o - r_{33}\Gamma n_o^3}{r_{33}\Gamma n_o^3} + \frac{(r_{33}\Gamma n_o^3 + 2\Delta n_o)}{r_{33}\Gamma n_o^3}\cos\Delta\varnothing\right] + 1$$

$$\cos\Delta\varnothing = \frac{2I_1 r_{33}^2\Gamma^2 n_o^6 - I_2 r_{33}^2\Gamma^2 n_o^6 - 8\Delta n_o^2 I_2 - 4\Delta n_o I_2 r_{33}\Gamma n_o^3}{I_2\left(4\Delta n_o r_{33}\Gamma n_o^3 + 8\Delta n_o^2\right)} \tag{8}$$

$$\cos\Delta\varnothing = \frac{\left(2I_1 - I_2\right) r_{33}^2\Gamma^2 n_o^6}{I_2(4\Delta n_o r_{33}\Gamma n_o^3 + 8\Delta n_o^2)} - 1 \tag{9}$$

$$\cos\Delta\varnothing + 1 = \frac{\left(2I_1 - I_2\right) r_{33}^2\Gamma^2 n_o^6}{I_2(4\Delta n_o r_{33}\Gamma n_o^3 + 8\Delta n_o^2)} \tag{10}$$

$$\because \Delta\phi = \frac{\pi L n_o^3 r_{33} V}{\lambda d} \tag{11}$$

where V is the applied voltage in volt. Plugging Eq. (10) into Eq. (11) yields:

$$\Delta n_o = A \pm B \tag{12}$$

$$A = \frac{-\left(4I_2 r_{33}\Gamma n_o^3\cos\Delta\varnothing + 4I_2 r_{33}\Gamma n_o^3\right)}{16\left(1+\cos\Delta\varnothing\right)}$$

$$B = \frac{\sqrt[2]{\left(4I_2 r_{33}\Gamma n_o^3\cos\Delta\varnothing + 4I_2 r_{33}\Gamma n_o^3\right)^2 - 4\left(I_2 - 2I_1\right) r_{33}^2\Gamma^2 n_o^6\left(8 + 8\cos\Delta\varnothing\right)}}{16\left(1+\cos\Delta\varnothing\right)}$$

Eq. (12) expresses the fundamental model of Mach–Zehnder modulator (MZM) in the optical communication systems. The study was designed by selecting a longitudinal optical modulator in which the electric field is V/L, and the phase change is π (i.e., the polarities are not opposite). The study utilizes the relation between the changing of negative ordinary refractive index and the optical confinement factor as expressed in Eqs. (17) and (7). Hence, the designed system mathematical model is presented as in Eq. (12). The study was carried out when the large change in the ordinary negative refractive index due to large confinement factor (i.e, large overlap). The data were analyzed through a proposed mathematical model to explain the relationship between the changing of the ordinary negative refractive index –Δno and the confinement factor Γ, as Eq. (12).

Results and discussion

In this paper, an analytical model is proposed to enhance the optical confinement factor of the MZM based on the material of LN. The performance of the proposed modulator can be estimated by employing Eq. (12) where the techniques of electro-optic effect and electro-refractive are considered. The large energy of the optical light (i.e., high energy of light intensity) is merged with the electrical field to shape large ball lightning into the inner waveguide. The high modulation of light intensity of the modulator depends on how strong the ball lightning is and that indicates the high performance of modulating that light intensity in the modulator. Thus, the phenomena of a ball lightning are

named as the overlap due to the overlapping between the electric field and the optical light where the large ball light is called big overlap (i.e., large optical confinement factor). Therefore, the large relative refractive index variation indicates a large overlap (i.e., large optical confinement factor). In this paper, it is shown that the ordinary negative change in the refractive index (Δn_o) is affected by applying an electric field (E) at a value of 4V/μm. This can be even better when the larger ordinary negative change in the refractive index is associated with as small length as 3–8 μm of the waveguide branch which consequently leads to a large optical confinement factor (large overlap). This emphasizes how vital it is to select a suitable length of arms with respect to the applied electric field with a large negative ordinary change in the refractive index Δn_o, as shown in Figures 5 and 6. Furthermore, the refractive index and electro-optic coefficient change with an ordinary negative change in refractive index Δn_o for LN where the length of the branch is an effective factor to shape the required large ball lightning ,as shown in Figures 7 and 8. In addition, a better change in the ordinary negative of refractive index Δno can be obtained when using a window (near-infrared–visible) optical wavelength which has improved the modulation performance of MZM as presented in Figure 9.

In 2020, Qi and Li (2020) and in 2019 He et al. (2019), designed the integrated electro-optical devices such as the modulator using a high refractive index to increase the optical confinement factor where the lengths of the modulator's arms are 3 mm, and 13 mm while the waveguide lengths are 0.62 cm, 1.86 cm, and 4.43 cm. Because the length of the arm is large (in mm), the changing of the refractive index is small. adding the electric field induced using a phase change is π/2 (i.e, opposite polarities). Moreover, transverse type modulator is used where the applied electric field is (Maldonado, 1995):

$$E = \frac{V}{d} \tag{13}$$

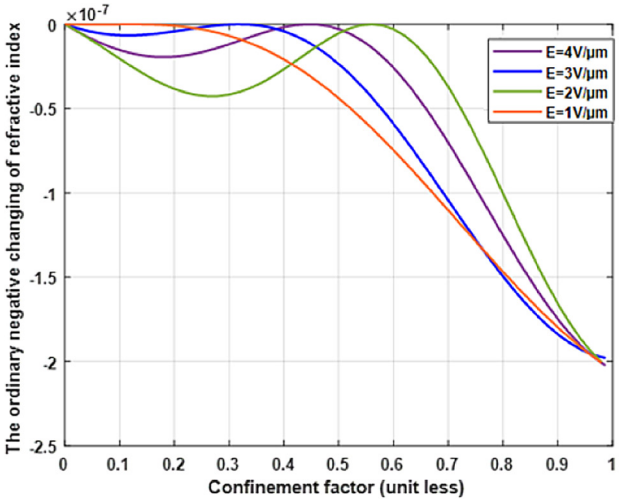


Figure 6: The ordinary negative changing of refractive index as a function of the confinement factor under different intensity of the applied electrical field.

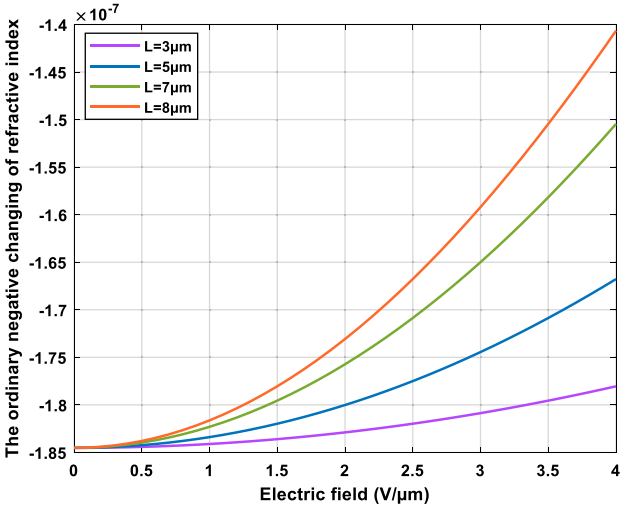


Figure 5: The ordinary negative changing of refractive index by applying electric field versus different lengths of arms.

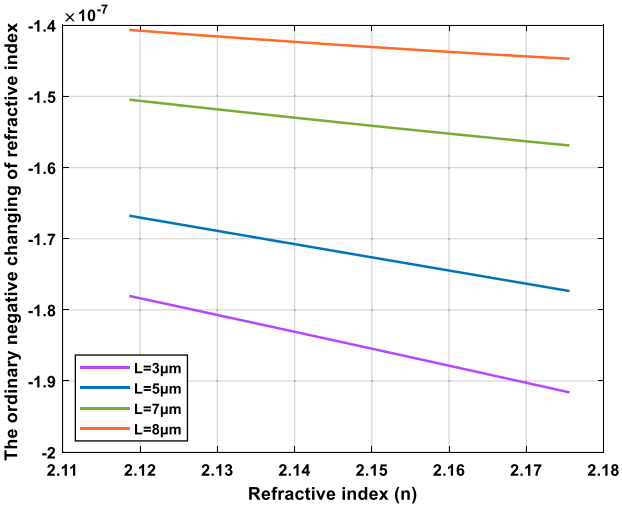


Figure 7: The ordinary negative changing of refractive index as a function of refractive index versus different lengths of arms for $LiTaO_3$.

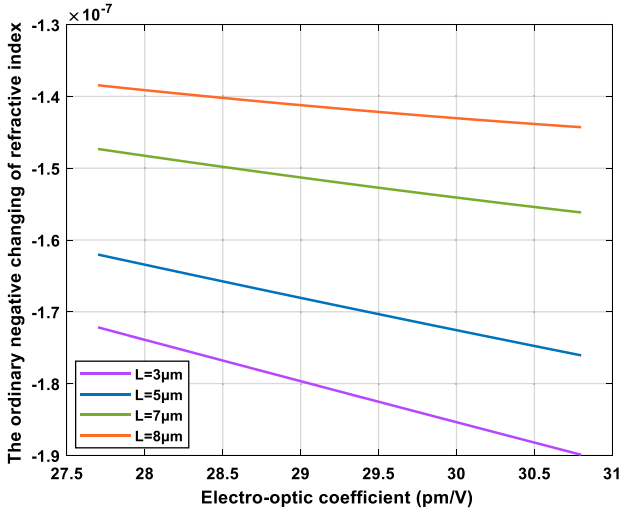


Figure 8: The ordinary negative changing of refractive index as a function of electro-optic coefficient versus different lengths of arms for $LiTaO_3$.

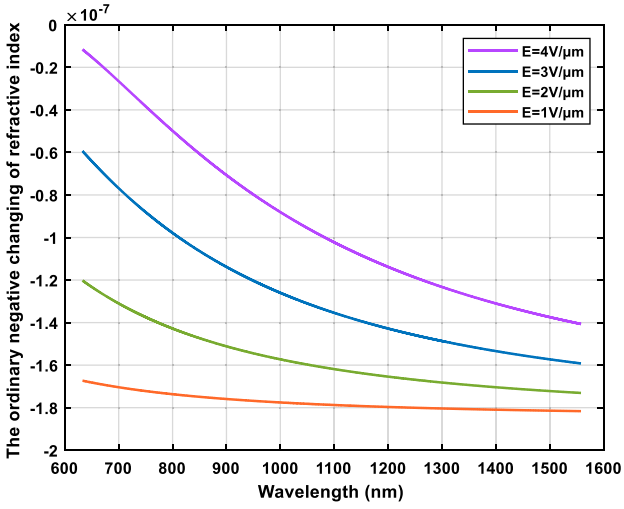


Figure 9: The ordinary negative changing of refractive index with wavelength under different applied electric fields for $LiTaO_3$.

where d is the waveguide electrode spacing which is directly proportional to the confinement factor. The confinement factor can be slightly degraded by decreasing the waveguide electrode spacing d as expressed in the following equations (Hagn, 2001; Maldonado, 1995):

$$\Delta n_o = -\frac{n^3 r_{13} \Gamma V}{2d} \tag{14}$$

where r_{13} is the electro-optic coefficient.

$$Pm/V, \Gamma = \frac{2\pi \Delta n L}{\lambda} \tag{15}$$

In this paper, used a small waveguide electrode spacing d and focused in this paper on the waveguide electrode spacing d, thus, a large ordinary changing of refractive index Δn, then a large confinement factor.

Thus, in this paper, the electro-optic modulator is designed using a high refractive index that induces a large confinement factor. The proposed design has deployed a longitudinal modulator type in which the applied electric field can be evaluated by (Maldonado, 1995):

$$E = \frac{V}{L} \tag{16}$$

where L is the length of the modulator arm in μm where the used values of L in the proposed design are 3 μm, 5 μm, 7 μm, and 8 μm. Since the proposed structure adopts small lengths of arm (in μm), the change in the refractive index Δn is large and hence the confinement factor is large as well based on the following formula (Hagn, 2001):

$$\Delta n_o = -\frac{n^3 r_{13} \Gamma V}{2L} \tag{17}$$

Furthermore, the electric field induces using a phase change is π (i.e, polarities not opposite), where it selects a suitable electric field, that induces a large changing of refractive index. Eventually, the main benefit of this work is the enhancement of the confinement factor as well as the improvement in the modulation efficiency of the modulator, see Table 2.

In the presented results, the longitudinal configuration of the separation distance between arms (d) does not have any effect on the electric field because L and d are equal (Maldonado, 1995), thus the electric field E is restricted. Finally, the future work is to experimentally assemble this design.

The challenges and difficulties of this design are in the selection of the values of variables such as the length of the modulator arm (L) and the separation distance between arms (d) in micrometers because of a small applied electric field E through the small area of these arms (i.e., $E < 10$ V/μm). Meantime, a large applied electric field (E) is not feasible here because the design is limited by small size whereas for commercial modulators, E can be hundreds of voltages per millimeter with a big size of the available systems in mm or even in cm. Therefore, in the longitudinal

Table 2. The comparison between the reference paper (Chang et al., 2017; Qi and Li, 2020) and this work.

Reference	Δn	L	d	$\Delta\emptyset$	E	Γ	Modulator type
(Qi and Li, 2020) and (He et al., 2019)	Large	Large In mm	Small	$\pi/2$	$E = V/d$	Large	Transvers
This work	Large	Small In μm	–	π	$E = V/L$	Large	Longitudinal

configuration, the electric field E is restricted because ($L = d$), and the electric field ($E = V/L$). As a result, the aspect ratio (L/d) is unity and d is not controlled by the electric field E. On the other hand, in the transverse configuration, the electric field is not restricted as ($d \ll$ L), and d operates as a capacitor in the device. Therefore, a reduction in d due to the electric field E has increased the aspect ratio (L/d) and hence d is controlled by E, where L is also large.

Conclusions

The proposed structure has accomplished good performance with large optical confinement factor resulting from as small as 8 μm length of arms which consequently led to a compact MZM. The large ordinary negative changing of the refractive index when applying lower driving power of the electric field of 1–4 V/μm to the MZM has reflected better performance. With LN, the best length of arms was about 8 μm with a large negative change in the refractive index when using near-infrared and visible wavelengths with the electric field of 4V/μm.

Literature Cited

Akhtar, M. B. 2022. The use of a convolutional neural network in detecting soldering faults from a printed circuit board assembly. *HighTech and Innovation Journal* 3(1): 1–14.

Alexander, K., George, J. P., Verbist, J., Neyts, K., Kuyken, B., Van Thourhout, D. and Beeckman, J. 2018. Nanophotonic Pockels modulators on a silicon nitride platform. *Nature communications* 9(1): 3444.

Bea, S. and Teich, M. 1991. *Fundamentals of photonics*, Wiley, New York, p. 313.

Boes, A., Corcoran, B., Chang, L., Bowers, J. and Mitchell, A. 2018. Status and potential of lithium niobate on insulator (LNOI) for photonic integrated circuits. *Laser & Photonics Reviews* 12(4): 1700256.

Cai, L., Kang, Y. and Hu, H. 2016. Electric-optical property of the proton exchanged phase modulator in single-crystal lithium niobate thin film. *Optics Express* 24(5): 4640–4647.

Casson, J. L., Gahagan, K. T., Scrymgeour, D. and Jain, R. K. 2004. Electro-optic coefficients of lithium tantalate at near-infrared wavelengths. *JOSA B* 21(11): 1948–1952.

Chang, L., Pfeiffer, M. H. P., Volet, N., Zervas, M., Peters, J. D., Manganelli, C. L., Stanton, E. J., Li, Y., Kippenberg, T. J. and Bowers, J. E. 2017. Heterogeneous integration of lithium niobate and silicon nitride waveguides for wafer-scale photonic integrated circuits on silicon. *Optics Letters* 42(4): 803–806.

Chang, L., Li, Y., Volet, N., Wang, L., Peters, J. and Bowers, J. E. 2016. Thin film wavelength converters for photonic integrated circuits. *Optica* 3(5): 531–535.

Chen, L., Xu, Q., Wood, M. G. and Reano, R. M. 2014. Hybrid silicon and lithium niobate electro-optical ring modulator. *Optica* 1(2): 112–118.

Deshpande, R., Zenin, V. A., Ding, F., Mortensen, N. A. and Bozhevolnyi, S. I. 2018. Direct characterization of near-field coupling in gap plasmon-based metasurfaces. *Nano Letters* 18(10): 6265–6270.

DeVault, C. T., Zenin, V. A., Pors, A., Chaudhuri, K., Kim, J., Boltasseva, A., Shalaev, V. M. and Bozhevolnyi, S. I. 2018. Suppression of near-field coupling in plasmonic antennas on epsilon-near-zero substrates. *Optica* 5(12): 1557–1563.

Figura, C. C. 2000. Second order nonlinear optics in ionically self-assembled thin films. PhD Dissertation, Virginia Tech.

Girouard, P., Chen, P., Jeong, Y. K., Liu, Z., Ho, S. and Wessels, B. W. 2017. X-2 modulator with 40-GHz modulation utilizing $BaTiO_3$ photonic crystal waveguides. *IEEE Journal of Quantum Electronics* 53(4): 1–10.

Guarino, A., Poberaj, G., Rezzonico, D., Degl'Innocenti, R. and Günter, P. 2007. Electro–optically tunable microring resonators in lithium niobate. *Nature Photonics* 1(7): 407–410.

Hagn, G. 2001. Electro-optic effects and their application in indium phosphide waveguide devices for fibre optic access networks. PhD dissertation, ETH Zurich.

He, M., Xu, M., Ren, Y., Jian, J., Ruan, Z., Xu, Y., Gao, S., Sun, S., Wen, X., Zhou, L., Liu, L., Guo, C., Chen, H., Yu, S., Liu, L. and Cai, X. 2019. High-performance hybrid silicon and lithium niobate Mach–Zehnder modulators for 100 Gbit s^{-1} and beyond. *Nature Photonics* 13(5): 359–364.

Janner, D., Tulli, D., García-Granda, M., Belmonte, M. and Pruneri, V. 2009. Micro-structured integrated electro-optic LiNbO3 modulators. *Laser & Photonics Reviews* 3(3): 301–313.

Jin, S., Xu, L., Zhang, H. and Li, Y. 2015. $LiNbO_3$ thin-film modulators using silicon nitride surface ridge waveguides. *IEEE Photonics Technology Letters* 28(7): 736–739.

Korkishko, Y. N., Fedorov, V., De Micheli, M., Baldi, P., El Hadi, K. and Leycuras, A. 1996. Relationships between structural and optical properties of proton-exchanged waveguides on Z-cut lithium niobate. *Applied Optics,* 35(36): 7056–7060.

Lu, H., Sadani, B., Ulliac, G., Courjal, N., Guyot, C., Merolla, J.-M., Collet, M., Baida, F. I. and Bernal, M.-P. 2012a. 6-micron interaction length electro-optic modulation based on lithium niobate photonic crystal cavity. *Optics Express* 20(19): 20884–20893.

Lu, H., Sadani, B., Courjal, N., Ulliac, G., Smith, N., Stenger, V., Collet, M., Baida, F. I. and Bernal, M.-P. 2012b. Enhanced electro-optical lithium niobate photonic crystal wire waveguide on a smart-cut thin film. *Optics Express* 20(3): 2974–2981.

Luff, B. J., Wilkinson, J. S., Piehler, J., Hollenbach, U., Ingenhoff, J. and Fabricius, N. 1998. Integrated optical Mach–Zehnder biosensor, in. *Journal of Lightwave Technology* 16(4): 583–592.

Maldonado, T. A. 1995. Electro-optic modulators. *Handbook of optics* 2: 13–11.

Mercante, A. J., Shi, S., Yao, P., Xie, L., Weikle, R. M. and Prather, D. W. 2018. Thin film lithium niobate electro-optic modulator with terahertz operating bandwidth. *Optics Express* 26(11): 14810–14816.

Poberaj, G., Hu, H., Sohler, W. and Guenter, P. 2012. Lithium niobate on insulator (LNOI) for micro-photonic devices. *Laser & photonics reviews* 6(4): 488–503.

Priscilla, S. J., Judi, V. A., Daniel, R. and Sivaji, K. 2020. Effects of chromium doping on the electrical properties of ZnO nanoparticles. *Emerging Science Journal* 4(2): 82–88.

Qi, Y. and Li, Y. 2020. Integrated lithium niobate photonics, *Nanophotonics,* 9(6): 1287–1320.

Rao, A., Patil, A., Rabiei, P., Honardoost, A., DeSalvo, R., Paolella, A. and Fathpour, S. 2016. High-performance and linear thin-film lithium niobate Mach–Zehnder modulators on silicon up to 50 GHz. *Optics Letters* 41(24): 5700–5703.

Rao, A. and Fathpour, S. 2017. Compact lithium niobate electrooptic modulators. *IEEE Journal of Selected Topics in Quantum Electronics* 24(4): 1–14.

Roussey, M., Baida, F. I. and Bernal, M.-P. 2007. Experimental and theoretical observations of the slow-light effect on a tunable photonic crystal. *JOSA B* 24(6): 1416–1422.

Roussey, M., Bernal, M.-P., Courjal, N., Van Labeke, D., Baida, F. and Salut, R. 2006. Electro-optic effect exaltation on lithium niobate photonic crystals due to slow photons. *Applied physics letters* 89(24): 241110.

Scharnberg, A. A., de Loreto, A. C. and Alves, A. K. 2020. Optical and structural characterization of Bi2FexNbO7 nanoparticles for environmental applications. *Emerging Science Journal* 4(1): 11–17.

Sulser, F., Poberaj, G., Koechlin, M. and Günter, P. 2009. Photonic crystal structures in ion-sliced lithium niobate thin films. *Optics Express* 17(22): 20291–20300.

Tavlykaev, R. F. and Ramaswamy, R. V. 1999. Highly linear Y-fed directional coupler modulator with low intermodulation distortion. *Journal of Lightwave Technology* 17(2): 282.

Thomaschewski, M., Zenin, V. A., Wolff, C. and Bozhevolnyi, S. I. 2020. Plasmonic monolithic lithium niobate directional coupler switches. *Nature Communications* 11(1): 1–6.

Wang, C., Zhang, M., Chen, X., Bertrand, M., Shams-Ansari, A., Chandrasekhar, S., Winzer, P. and Lončar, M. 2018. Integrated lithium niobate electro-optic modulators operating at CMOS-compatible voltages. *Nature* 562(7725): 101–104.

Wang, X., Weigel, P. O., Zhao, J., Ruesing, M. and Mookherjea, S. 2019. Achieving beyond-100-GHz large-signal modulation bandwidth in hybrid silicon photonics Mach Zehnder modulators using thin film lithium niobate. *APL Photonics* 4(9): 096101.

Weigel, P. O., Zhao, J., Fang, K., Al-Rubaye, H., Trotter, D., Hood, D., Mudrick, J., Dallo, C., Pomerene, A. T., Starbuck, A. L., DeRose, C. T., Lentine, A. L., Rebeiz, G. and Mookherjea, S. 2018. Bonded thin film lithium niobate modulator on a silicon photonics platform exceeding 100 GHz 3-dB electrical modulation bandwidth. *Optics Express* 26(18): 23728–23739.

Wooten, E. L., Kissa, K. M., Yi-Yan, A., Murphy, E. J., Lafaw, D. A., Hallemeier, P. F., Maack, D., Attanasio, D. V., Fritz, D. J., McBrien, G. J. and Bossi, D. E. 2000. A review of lithium niobate modulators for fiber-optic communications systems. *IEEE Journal of Selected Topics in Quantum Electronics* 6(1): 69–82.

Xu, M., Chen, W., He, M., Wen, X., Ruan, Z., Xu, J., Chen, L., Liu, L., Yu, S. and Cai, X. 2019. Michelson interferometer modulator based on hybrid silicon and lithium niobate platform. *APL Photonics* 4(10): 100802.

Xu, M., He, M., Zhang, H., Jian, J., Pan, Y., Liu, X., Chen, L., Meng, X., Chen, X., Li, Z., Xiao, X., Yu, S. and Cai, X. 2020. High-performance coherent optical modulators based on thin-film lithium niobate platform. *Nature Communications* 11(1): 1–7.

Yi-Yan, A. 1983. Index instabilities in proton-exchanged LiNbO3 waveguides. *Applied Physics Letters,* 42,(8): 633–635.

Zenin, V. A., Choudhury, S., Saha, S., Shalaev, V. M., Boltasseva, A. and Bozhevolnyi, S. I. 2017. Hybrid plasmonic waveguides formed by metal coating of dielectric ridges. *Optics Express* 25(11): 12295–12302.

Zenin, V. A., Volkov, V. S., Han, Z., Bozhevolnyi, S. I., Devaux, E. and Ebbesen, T. W. 2012. Directional coupling in channel plasmon-polariton waveguides. *Optics Express* 20(6): 6124–6134.